ISSN 1063-7737, Astronomy Letters, 2007, Vol. 33, No. 3, pp. 182–191. © Pleiades Publishing, Inc., 2007.
Original Russian Text © O.G. Badalyan, V.N. Obridko, 2007, published in Pis'ma v Astronomicheskiĭ Zhurnal, 2007, Vol. 33, No. 3, pp. 210–220.

To the Problem of Solar Coronal Heating

O. G. Badalyan* **and V. N. Obridko**

Pushkov Institute of Terrestrial Magnetism, Ionosphere, and Radiowave Propagation, Russian Academy of Sciences, Troitsk, Moscow oblast, 142190 Russia

Received September 11, 2006

Abstract—We consider the adequacy of various solar coronal heating models. We show that the correlation between the intensity of the coronal Fe XIV 530.5 nm green line and the calculated magnetic field strength in the solar corona can be a useful tool for this purpose. We have established this correlation for coronal structures and magnetic fields of large spatial and temporal scales. The correlation found exhibits a strong dependence on both solar cycle phase and heliolatitude. The efficiency of a particular coronal heating mechanism is probably determined by the relative area occupied by low and high loops (including open structures). The direct current models based on slow field dissipation (DC) and the wave models based on Alfvén and magnetosonic wave dissipation (AC) are more efficient in the equatorial and polar zones, respectively.

PACS numbers : 96.60.Hv; 96.60.P-; 96.60.Q-; 96.60.Tf
DOI: 10.1134/S106377370703005X

Key words: *Sun, solar corona, coronal green line, magnetic fields, coronal heating.*

INTRODUCTION

The theory of solar and stellar coronal heating is still an important, outstanding problem of astrophysics. By now a large number of coronal heating mechanisms have been suggested and considered in detail (see Golub and Pasachoff 1997; Mandrini et al. 2000; Klimchuk 2002; Ulmschneider 2003; Aschwanden 2004). Thus, for example, Mandrini et al. (2000) cited 22 possible scaling laws for various heating mechanisms in their review paper. The choice of a specific model cannot be made, because there are probably several realistic coronal heating mechanisms and the role of these mechanisms is different in different regions (active regions, the quiet Sun, coronal holes). This, in turn, is most likely determined by the contribution from fields of various scales, their internal structure, the combination of low and high loops, and the contribution from open magnetic fields. Therefore, quantitative estimations of the correlation between solar coronal emission characteristics and magnetic fields are required to elucidate the mechanisms of the magnetic field effect on physical processes in the corona.

The correlation between the characteristics of the coronal Fe XIV 530.5 nm green line emission and those of the magnetic field seems promising for solving the coronal heating problem. The emission in this line characterizes the level of activity in the solar corona. Dense loops and clusters of loops in the inner corona are the regions of the most intense green line emission. A loop temperature of ~2 MK is the most commonly encountered temperature of the lower corona. A balance between the energy inflow and outflow in loops is believed to be established precisely at this temperature. A density increase in loops causes the green line emission to be enhanced, since its intensity is proportional to the square of the density. The regions of reduced green line emission are genetically related to coronal holes (see, e.g., Fisher and Musman 1975; Letfus et al. 1980; Sýkora 1992; Guhathakurta et al. 1996), i.e., to regions of open magnetic configurations. A big advantage of the index that characterizes the green line emission is that it is determined almost simultaneously for all heliolatitudes. Thus, the green line allows the field effect to be studied both in equatorial, closed configurations and in open regions like coronal loops.

There are a few papers in which the coronal green line emission is correlated with the magnetic field (see, e.g., Guhathakurta et al. 1993; Wang et al. 1997; Rušin and Rybanský 2002). Wang et al. (1997) showed that the density at the footpoints of magnetic field tubes is related to the magnetic field strength by $n_{\rm foot} \propto \langle B_{\rm foot}\rangle^{0.9}$. Relations of this type are considered in several theoretical works. Previously (Badalyan and Obridko 2004, 2006), we correlated the spatial distribution of the coronal Fe XIV

*E-mail: badalyan@izmiran.troitsk.ru

530.5 nm green line intensity I with the magnetic field strength B and its components over the period 1977–2001 (solar cycles 21, 22, and (current) 23). The correlation between B and I was found to be complex and to depend on heliolatitude and cycle phase.

In this paper, we compare the observed patterns of correlation between the coronal green line intensity and the magnetic field strength in various latitude zones with the results of theoretical calculations for several solar coronal heating models. Our analysis is aimed at studying the large-scale structure of the slowly changing corona. Our comparison with theoretical models was made for solar minimum, when the situation is relatively simple and all patterns manifest themselves most clearly. Our calculations show that we cannot choose a unified model that would adequately describe the coronal heating in the low-latitude zone with a large number of dense coronal loops and in the polar zone where structures with an open magnetic configuration largely dominate.

OBSERVATIONAL DATA AND THE METHOD OF CALCULATION

To analyze the quantitative correlation between the coronal Fe XIV 530.5 nm green line intensity and the coronal magnetic field strength and its components, we calculated the cross-correlation between the corresponding synoptic charts for the period 1977–2001 (Badalyan and Obridko 2004, 2006).

Based on patrol observations at several coronal stations reduced to a single photometric system, we mapped the green line intensity distribution. Here, we use the database created by J. Sýkora. The process of data homogenization (i.e., reduction to a single system) was described by Sýkora (1971). A detailed description of the database can be found in Storini and Sýkora (1997) and Sýkora and Rybák (2005). In this database, the green line intensities are given in absolute coronal units (a.c.u.) with a longitude step of ~13° (one day) and a latitude step of 5° (1 a.c.u. is one millionth of the intensity of the solar disk center in a 0.1-nm band of the continuum adjacent to the line). The data for the days without observations were interpolated (about 15%). All of the data were reduced to a height of 60″ above the limb. Using our maps, we made a movie that is a visualization of the data on the spatiotemporal coronal green line intensity distribution (Badalyan et al. 2004, 2005). The movie and additional materials are accessible at http://helios.izmiran.rssi.ru/hellab/Badalyan/green/.

The coronal magnetic field strength was calculated in the potential approximation based on Wilcox Solar Observatory observations at the photospheric level (the data were retrieved from the Internet, http://quake.stanford.edu/~wso/wso.html). We calculated the coronal magnetic field using a well-known method described by Hoeksema and Scherrer (1986) and Hoeksema (1991). For this work, we used a code that allowed all of the magnetic field components to be calculated for any distance from the photospheric surface to the source surface (Kharshiladze and Ivanov 1994). The magnetic field can be calculated for any time; in our calculations, this is the data of passage through the central meridian. Both the original observations and the calculated data on the magnetic field are bounded by a ±70° latitude zone. The results of our calculations are presented in the form of a grid, 80 points in longitude by 100 points in latitude, i.e., the synoptic chart for each rotation has a longitude step of 4.°5 and a latitude step of 1.°4. For the subsequent analysis, we calculated the total magnetic field strength $B = \sqrt{B_t^2 + B_r^2}$, where B_t and B_r are the tangential and radial magnetic field components, respectively. The calculations were performed for a distance of $1.1R_\odot$ close to the height of 60″ to which the data on the coronal green line intensity in the database used were reduced. In our calculations, we performed the summation over ten harmonics and applied a polar correction that takes into account the insufficient reliability of magnetic field measurements near the poles (Obridko and Shelting 1999).

The observational data on the green line and the calculated magnetic field were averaged over six consecutive Carrington rotations. These maps smoothed over six rotations allow large-scale long-lived coronal structures at the green line emission height to be traced. The data on the green line intensity and the magnetic field organized in this way have an effective spatial resolution of about 15°. For such a large temporal averaging, the dynamic phenomena for which the potential approximation is no longer valid are virtually excluded from our consideration.

TWO TYPES OF CORRELATION BETWEEN THE CORONAL GREEN LINE INTENSITY AND THE MAGNETIC FIELD

For a quantitative expression of the correlation between the green line intensity and the magnetic field strength, we calculated the correlation coefficients r_B between these parameters at those points of the synoptic charts for which the green line intensities were given in the database (i.e., with steps of 13° in longitude and 5° in latitude). The behavior of the correlation coefficient r_B was studied in two latitude zones: in the low-latitude sunspot formation zone

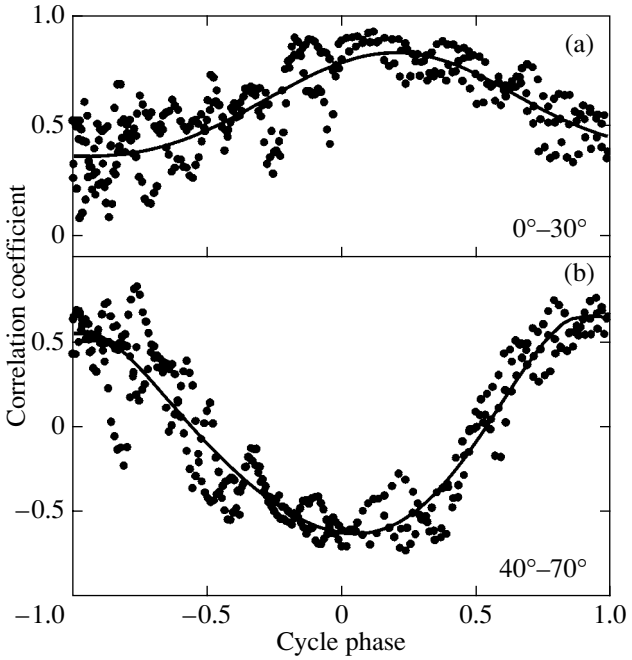

Fig. 1. Correlation coefficients between the coronal green line intensity and the magnetic field strength in the sunspot formation zone (a) and the high-latitude zone (b) vs. solar cycle phase.

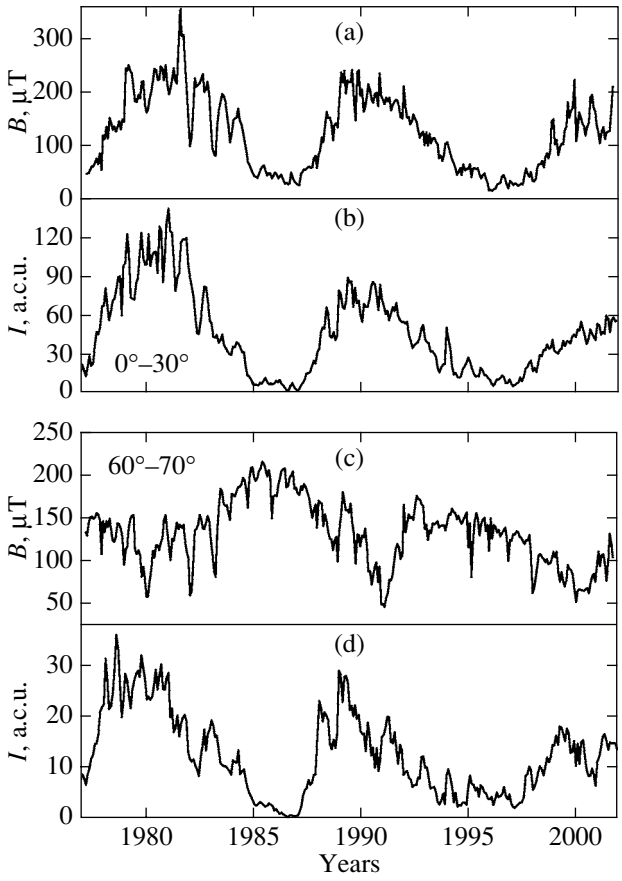

Fig. 2. Green line intensity and magnetic field strength vs. time in the sunspot formation zone (a, b) and the polar zone (c, d).

$|\varphi| \le 30°$ and in the zone $|\varphi| > 40°$, which below we will arbitrarily call a high-latitude zone (the northern and southern hemispheres are combined). The total number of points in each of these zones is approximately equal to 400. This gives a mean error in each correlation coefficient of 0.02–0.03 and this error does not exceed 0.05 even at low values of the coefficient (for the details of our calculations, see Badalyan and Obridko 2004, 2006).

The correlation coefficients r_B calculated separately for the sunspot formation zone $|\varphi| \le 30°$ and the higher-latitude zone were found to exhibit a distinct cyclic pattern. In Figs. 1a and 1b, the coefficients r_B for the sunspot formation zone and the high-latitude zone are plotted against the cycle phase Φ. By the definition of Mitchell (1929), the cycle phase was calculated as $\Phi = (\tau - m)/(|M - m|)$, where τ is the current time and M and m are the times of the nearest maximum and minimum of the 11-year solar cycle, respectively. At the cycle minimum $\Phi = 0$, the phase is positive on the rise branch and negative on the decline branch. Figure 1 shows that the r_B variations in the sunspot formation zone and the higher-latitude zone are in antiphase. In the low-latitude zone, the sign of the correlation coefficient r_B is always positive. Here, it reaches the highest values at the cycle minimum and decreases significantly at the maximum. In contrast, in the zone of middle and high latitudes, r_B reaches the highest positive values at the cycle maximum and approximately the same (in absolute value), but negative values at the cycle minimum. The coefficient r_B passes through zero in the high-latitude zone approximately at the beginning of the rise branch and at the end of the decline branch of the solar cycles.

It may be concluded that there is a completely different correlation between the green line intensity and the magnetic field at low and high latitudes in the corona. The variation of this correlation with time is cyclic in pattern.

The behavior of the green line intensity and the magnetic field strength in an activity cycle is also different in different latitude zones. In Fig. 2, the green line intensity (in a.c.u.) and the magnetic field strength are plotted against time for two latitude zones. In Figs. 2a and 2b, these time dependences are given for the sunspot formation zone $|\varphi| \le 30°$. We see that the green line intensity and the magnetic field

strength vary with time in a similar way. The two parameters under discussion increase at the maximum and decrease at the minimum.

Figures 2c and 2d show the behavior of these parameters in the polar zone $|\varphi| = 60°–70°$. Here, the green line intensity and the magnetic field strength vary in antiphase. The green line intensity, as at all other latitudes, increases at the cycle maximum and decreases at the minimum. In contrast, the magnetic field decreases at the cycle maximum and increases at the minimum. The large-scale magnetic field, which varies with solar cycle precisely in this way, is known to dominate at high latitudes. The fact that the green line intensity varies in antiphase with the large-scale magnetic field can be explained as follows. At high latitudes, it is the large-scale magnetic field that affects significantly the formation of green line emission conditions, i.e., the formation of "structures" with green line emission; for example, a stronger large-scale field favors the formation of rarefied regions like coronal holes. The green line emission in such structures is weaker due to a reduction in temperature and density in them. An increase in the strength of the large-scale polar field gives rise to a larger number of structures with an open magnetic configuration.

The correlation of the green line intensity with the magnetic field strength and its components can be represented as a functional dependence. Near solar minimum, when the magnetic field has a relatively simple structure, the correlation between the green line intensity and the magnetic field strength for the two latitude zones under consideration can be represented by a power law of the type

$$I \propto B^q. \quad (1)$$

Figure 3 shows examples of this correlation. For the sunspot formation zone, the regression shown in Fig. 3a is described by the formula $I = 0.314 \times B^{0.896}$. The set of points in this figure refers to the corresponding synoptic chart constructed from the data averaged over rotations 1783–1788 ($13 \times 27 = 351$ points). This is the beginning of 1987, i.e., the beginning of an activity rise in cycle 22. For other cases, shortly before and immediately after the solar minima, the index q is also positive and varies within the range from 0.75 to 1.00.

For the zone $|\varphi| = 40°–70°$, the sign of the power-law index q is negative during the minimum. In Fig. 3b, this dependence is shown for the synoptic chart constructed for rotations 1777–1782. This is 1986, the minimum of cycle 21. Here, the dependence is satisfactorily fitted by the formula $I = 71B^{-0.644}$. We see that the magnetic field strength here is approximately twice as large as that in the low-latitude zone (upper panel). In contrast, the green line intensity is very low. Therefore, Fig. 3b shows the values averaged over six Carrington rotations for each latitude with a 5° step separately for the northern and southern hemispheres (the pairs of points in the plot). We see that the magnetic field strength increases significantly with latitude and approaches 250 μT at a latitude of 70° (the extreme right pair of points). Although the uncertainty of each individual recording is large, the coronal green line intensity at high latitudes in the period of low activity and, accordingly, weak coronal emission in this line, the power-law fit with a negative index is determined here fairly reliably (the total number of initial values from which the intensity is determined at each point in the lower plot is 162). For other charts of the solar minimum, the power-law index q varies within the range from -0.6 to -0.8.

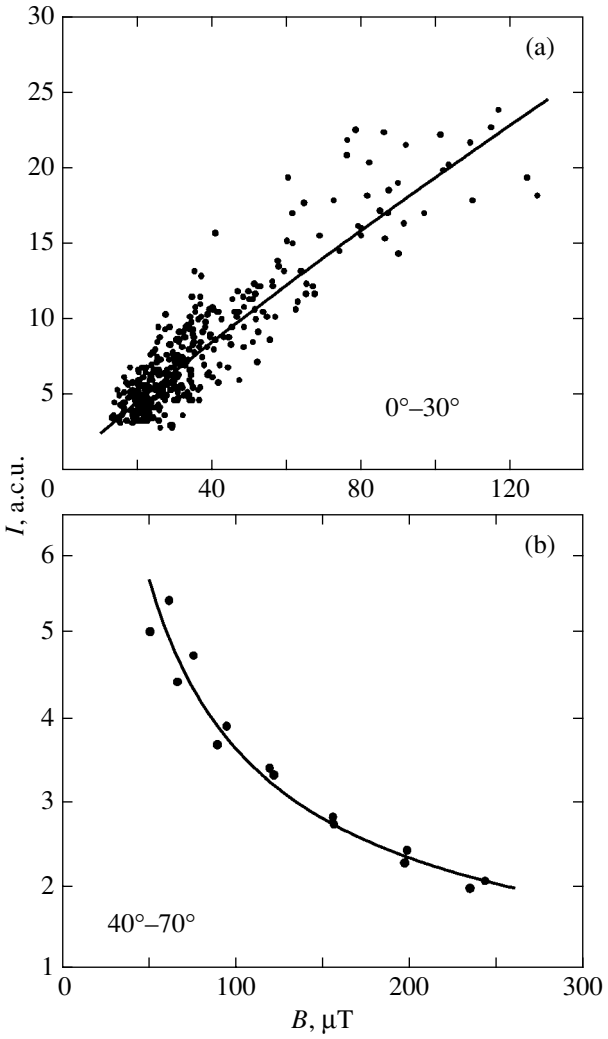

Fig. 3. Correlation between the coronal green line intensity and the magnetic field strength in the sunspot formation zone (a) and the high-latitude zone (b).

COMPARISON OF THE RESULTS OBTAINED WITH CORONAL HEATING MODELS

Thus, the green line intensity in the equatorial zone increases almost linearly with magnetic field strength near solar minimum. In the high-latitude zone, the coronal green line intensity decreases as the magnetic field strength and its components increase at solar minimum. The correlation between the line intensity and the magnetic field in this zone can be described by a power law with a negative index. These conclusions allow us to compare the results obtained with various coronal heating models.

The thermal balance of the corona is determined by the relationship between the inflow of heat and its losses. In closed magnetic structures dominating in the sunspot formation zone, the energy balance is determined by heating, radiative losses, and thermal conduction. In most cases, the losses in moderately rarefied loops are determined mainly by radiation (Aschwanden 2004). Assuming that the coronal green line emission is proportional to the radiation flux from the corona, we can directly compare our results with heating models. Of course, the heating models are defined by a large number of parameters, but these are all interrelated and can be reduced to one independent parameter, in our case, to the magnetic field strength B.

The situation at high latitudes, where coronal holes, i.e., structures with an open magnetic configuration, dominate during the minimum, is slightly more complex. In this zone, the losses through the solar wind are larger than the radiative losses. Therefore, an increase in the solar wind velocity and in the area of coronal holes, which grow with an effective increase in the large-scale magnetic field, can cause a reduction in radiative losses and, accordingly, a reduction in coronal emission. However, as will be seen from the subsequent analysis, there are heating models that directly lead to a reduction in coronal brightness with growing magnetic field.

Let us consider this question in more detail. The scaling law in form (1) can be related to the scaling law of coronal heating via the following relation (see Mandrini et al. 2000):

$$H \propto B^a L^b \rho^c V^d R^e, \qquad (2)$$

where H is the effective coronal heating power, L is the loop length, ρ is the plasma density in the loop, and V is the transverse velocity at the base of the corona; the parameters a, b, c, d, and e for different models are given in Mandrini et al. (2000). The meaning of R was defined by Mandrini et al. (2000) not quite clearly; they only specified that R means the loop radius in some models and the characteristic length scale of the magnetic field variations in other models. For the subsequent analysis, the dependences $B \propto L^\delta$ and $\rho \propto L^\varepsilon$ must be known and, disregarding the model dependence of V and R, (2) can then be expressed as

$$H \propto L^\alpha. \qquad (3)$$

The dependence $B \propto L^\delta$ was suggested by Klimchuk and Porter (1995). Note that, in general, the scaling laws of this type are quite applicable to loops of any size, including those going high in the corona up to the source surface, in view of their generality.

Klimchuk and Porter (1995) showed that the three models they considered (a field twisted into a bundle, a curved field, and resonance absorption of Alfvén waves) are consistent with the SXT (Yohkoh) observations of the coronal emission only at $\delta = -0.5, 0$, and -2, respectively. Previously, Golub et al. (1980) obtained $\delta \approx -0.7$ from Skylab data.

Mandrini et al. (2000) used an experimental value of α to compare the theory with observations. They calculated a theoretical value of α using (2) for 22 different coronal heating models and compared it with the experimentally found $\alpha = -2.0$ (Klimchuk and Porter 1995). In their calculations, they took $\delta = -0.88 \pm 0.3$ and $\varepsilon = -0.90$. The models based on slow field dissipation, or the *current* models (DC), give values of α that differ significantly from its observed values (from -3.0 to -4.0). The wave models (AC) based on the dissipation of Alfvén and magnetosonic waves give α from -3 to 1.5.

We correlated other parameters, more specifically, the coronal green line intensity and the magnetic field strength. Thus, we have an experimental value of q from (1). However, it turned out that this quantity could be easily related to heating model parameters. If, as is customary, the coronal green line intensity is assumed to be proportional to heating, then it follows from Eqs. (1)–(3) that

$$q = \alpha/\delta = a + b/\delta + \varepsilon c/\delta. \qquad (4)$$

This makes it possible to independently check the various coronal heating models for adequacy using the derived relationship between the coronal green line intensity and the magnetic field strength. For this purpose, we calculated theoretical values of q for all of the models from Mandrini et al. (2000). For the subsequent comparison (see the table), we used the same assumptions as those from Mandrini et al. (2000), i.e., $\delta = -0.88$ and $\varepsilon = -0.90$, although, as will be seen from the subsequent analysis, these do not closely correspond to our low-resolution observations. For our calculations, we used the scaling laws in the form in which they are given in Mandrini et al. (2000) and retained the model numbering (the first column in the table). In addition, we added the model by Schrijver

List of scaling laws for various coronal heating models

Model number	Reference	Scaling law	Parameters	α	q	q_{LS}
DC models						
1	1	$B^2L^{-2}V^2\tau$	–	-3.76	4.27	1.88
2	2	$B^2L^{-1}V\tan\theta$	–	-2.76	3.14	1.38
3	3	$B^2L^{-2}VR\phi$	–	-3.76	4.27	1.38
4	4	$BL^{-2}\rho^{1/2}V^2R$	–	-3.33	3.78	1.17
5	5	$B^{3/2}L^{-3/2}\rho^{1/4}V^{3/2}R^{1/2}$	–	-3.045	3.46	1.27
6	6	$B^2L^{-2}V^2\tau\log R_m$	–	-3.76	4.27	1.88
7	7	$B^2L^{-2}V^2\tau S^{0.1}$	–	-3.76	4.27	1.88
8	8	$B^2L^{-2}V^2\tau$	–	-3.76	4.27	1.88
9	9	$B^2L^{-1}R^{-1}V_{\rm ph}^2\tau$	–	-2.76	3.14	1.13
10	10	$B^2L^{-2}V_{\rm ph}^2\tau$	–	-3.76	4.27	1.88
11	11	$B^{3/2}L^{-3/2}\rho^{1/4}V^{3/2}R^{1/2}$	–	-3.045	3.46	1.27
12	12	$B^{5/3}L^{-4/3}\rho^{1/6}V^{4/3}R^{1/3}$	–	-2.95	3.35	1.31
13	13	$B^{s+1}L^{-1-s}\rho^{(1-s)/2}V^{2-s}R^s$	$s=0.7, m=-1$	-3.331	3.79	1.32
14	–	–	$s=1.1, m=-2.5$	-3.813	4.33	1.36
23	19	–	–	-1.915 ± 0.7	2.18 ± 0.8	1.09 ± 0.35
AC models						
15	14	$B^{1+m}L^{-3-m}\rho^{-(1+m)/2}$	$m=-1$	-2.0	2.27	1.0
16	–	–	$m=-2$	-1.45	1.65	0.72
17	15	$B^{1+m}L^{-1-m}\rho^{-(1+m)/2}$	$m=-1$	0.0	0.0	0.0
18	–	–	$m=-2$	1.43	-1.62	-0.72
19	16	$B^{1+m}L^{-m}\rho^{-(m-1)/2}$	$m=-1$	0.10	-0.11	-0.05
20	–	–	$m=-2$	1.53	-1.74	-0.74
21	17	$BL^{-1}\rho^{1/2}V^2$	–	-1.43	1.62	0.72
22	18	$B^{5/3}L^{-4/3}R^{1/3}$	–	-3.10	3.52	1.38

References: 1—Sturrock and Uchida (1981), Berger (1991); 2—Parker (1988), Berger (1993); 3—Galsgaard and Nordlund (1997); 4—Parker (1983); 5—Parker (1983), a modified model; 6—van Ballegooijen (1986); 7—Hendrix et al. (1996); 8—Galsgaard and Nordlund (1996); 9—Aly and Amari (1997); 10—Heyvaerts and Priest (1984), Browning and Priest (1986), Vekstein et al. (1993); 11—Einaudi et al. (1996), Dmitruk and Gómez (1997); 12—Heyvaerts and Priest (1992), Inverarity et al. (1995), Inverarity and Priest (1995a); 13—Milano et al. (1997); 14—Hollweg (1985); 15—Oĭman et al. (1995), Ruderman et al. (1997); 16—Halberstadt and Goedbloed (1995); 17—Galsgaard and Nordlund (1996); 18—Inverarity and Priest (1995b); 19—Schrijver et al. (2004).

et al. (2004) under number 23 to the table. References to the corresponding publications are listed in the second column of the table.

Note that despite the seemingly great variety of models, the main scheme is common to all of them. The initial assumption in all models is that there is some form of motions at the footpoints of magnetic flux tubes. Sometimes these are slow random motions (Sturrock and Uchida 1981; Parker 1983; Berger 1991), sometimes the pattern of motions is prescribed in advance, for example, the rotation of the tube ends in opposite directions (Galsgaard and Nordlund 1997). The motions can be rather weak (turbulence) or fast and strong, up to the emergence of an additional magnetic flux, which can lead to nanoflares (Parker 1988; Dmitruk and Gómez 1997). Depending on the magnetic field structure and strength, the consequences of photospheric motions can be different. In low-lying closed loops in the equatorial zone, these motions lead to a deviation from potentiality and give rise to current sheets, stresses, and even more complex systems. The superpotential current energy will be released either continuously through dissipation, retaining the complexity of the structure (e.g., model 12 (Heyvaerts and Priest 1992; Inverarity et al. 1995; Inverarity and Priest 1995a) and model 13 (Milano et al. 1997)), or passing through a sequence of quasi-potential states (model 9 (Aly and Amari 1997) and model 10 (Heyvaerts and Priest 1984; Browning and Priest 1986; Vekstein et al. 1993)). In open structures and giant loops, the photospheric motions give rise to magnetosonic waves whose resonance absorption or Joule dissipation leads to coronal heating (model 15 (Ofman et al. 1995; Ruderman et al. 1997), model 16 (Halberstadt and Goedbloed 1995), and model 18 (Inverarity and Priest 1995b)). It should be kept in mind that the resonance absorption can be produced by Joule dissipation. The scaling laws and their parameters are given in the third and fourth columns of the table: R_m is the magnetic Reynolds number, θ is the angle between the twisted field lines at the outer edge of the neighboring flux tubes, ϕ is the critical twisting angle, and $V_{\rm ph}$ is the photospheric value of V (the tube velocity in the corona V is commonly assumed to be $V_{\rm ph}$).

The fifth column of the table lists the values of α that we calculated under the same assumptions as those from Mandrini et al. (2000). The quantitative values of this parameter obtained in this way are in complete agreement with those shown in Fig. 8c from Mandrini et al. (2000). Our calculated values of the model parameter q are given in the sixth column of the table.

It follows from the table that all of the DC (current) model give very high, strictly positive values of q. At the same time, the AC (wave) models can give both positive and negative values of q. Thus, for example, AC models 15 and 16 yield q equal to 2.27 and 1.65 (Hollweg 1985) and model 21 yields $q = 1.62$ (Galsgaard and Nordlund 1996); model 22 yields $q = 3.52$ (Inverarity and Priest 1995b). Model 18 considered by Ofman et al. (1995) and Ruderman et al. (1997) as well as the two wave models 19 and 20 described by Halberstadt and Goedbloed (1995) give negative values of q.

Thus, none of the models is consistent with the experimental values of q that we found. However, it should be kept in mind that we (Badalyan and Obridko 2006; and this paper) determined only the experimental parameter q. We took the model parameters needed for our calculations from other publications. Not all of the assumptions made by Mandrini et al. (2000) correspond to the observations of large-scale coronal structures that we used.

(1) The value of $\delta = -0.88$ used above was obtained by Klimchuk and Porter (1995) for loops of relatively small sizes comparable to those of an active region or smaller. The error in this quantity is ± 0.3. We operate with the large-scale field. For large scales, Mandrini et al. (2000) used $\delta = -2.0$.

(2) It is not quite clear why Mandrini et al. (2000) did not take into account the dependence on R in their calculations. Indeed, Klimchuk and Porter (1995) showed that the loop radii and lengths depend weakly on one another. However, this conclusion was reached when analyzing loops of small sizes. In low-resolution observations, the contribution from extended loops, for which the assumption of $R \propto L$ is quite acceptable, is taken into account.

(3) The dependence on ρ in most models is weak ($c \ll 1$) and, hence, the adopted value of ε affects weakly the calculations.

(4) The contribution from the transverse velocity V is difficult to estimate. It is possible that precisely this contribution is responsible for the previously found (Badalyan and Obridko 2006) difference in the correlation of the coronal brightness with the radial and tangential magnetic field components.

Therefore, we also calculated q_{LS} with $\delta = -2.0$ and using the relationship $R \propto L$. The values of q_{LS} obtained in this way are given in the last column of the table and shown in Fig. 4. The values of q and q_{LS} are indicated in the figure by the filled squares and open circles, respectively. The domains of the power-law indices in (1) found from observations for the two latitude zones are shown in Fig. 4 by the horizontal gray bands.

The values of q_{LS} calculated in this way are considerably closer to the observed values of q. In the equatorial zone, the DC models with reconnection

in current sheets and at tangential discontinuities: 4 (Parker 1983), 9 (Aly and Amari 1997), 23 (Schrijver 2004), and the resonance AC models: 15 and 16 (Hollweg 1985), 17 (Galsgaard and Nordlund 1996), yield values of q_{LS} close to the observed ones. In the polar region, only the AC models (18 (Ofman et al. 1995; Ruderman et al. 1997) and 20 (Halberstadt and Goedbloed 1995)) correspond to the observations.

Two papers published already after the appearance of the review paper by Mandrini et al. (2000) should be noted.

Schrijver et al. (2004) assumed that $a = 1.04 \pm 0.3$ and $b = -1.0 \pm 0.5$ in Eq. (2), which corresponds to DC reconnection at tangential discontinuities. At the same time, Schrijver et al. (2004) disregarded the dependence on ρ, R, and V. At these values of a and b, taking (as was done by Mandrini et al. 2000) $\delta = -0.88$, we obtain α close to -2, in agreement with its experimental value (Mandrini et al. 2000). However, at this value of δ, the calculated q is 2.0 ± 1.0, which again is slightly higher than our experimental values of this parameter. Note that at higher (in magnitude) values of δ corresponding to the large-scale field, the calculated q_{LS} decrease and approach 1.0, i.e., the values of q that we obtained for the sunspot formation zone (see Fig. 4, model 23).

Warren and Winebarger (2006) directly correlated the coronal X-ray emission above active regions with the magnetic field strength and length of loops. It turned out that this correlation could be fitted by the formula $I \sim B^a L^b$. The best fit is achieved at $a = 1$ and depends weakly on b in a wide range of its values (from 0 to -2). This is consistent with our results for the equatorial zone (see Eq. (1) and Fig. 3a).

Thus, none of the mechanisms considered can explain the correlation between the coronal green line intensity and the magnetic field over the entire range of heliolatitudes in terms of a single model. It is believed that there is no unified coronal heating mechanism at all. Both the DC and AC mechanisms, which can lead to opposite (in sign) values of q, act in each zone on the Sun. Thus, the simultaneous action of these two mechanisms causes an effective decrease in the absolute value of q compared to its theoretical values. The contribution from these mechanisms depends on the structure and spatial sizes of the emitting region and on the magnetic field strength; it varies with latitude and cycle phase. It is believed that at minimum, when the field structure is simplest, the wave AC mechanisms and the DC mechanisms probably dominate in the high-latitude and equatorial zones, respectively.

Recall that the experimental parameter q in fitting formula (1) was determined from observations of large-scale coronal structures with low spatial and temporal resolutions. Therefore, the nonstationary processes leading to coronal heating were not directly taken into account in this paper. In addition, for such an averaging, the possible deviations from potentiality in the central parts of large active regions play no significant role. Note also that we basically equated the heating to the radiative losses. This is not quite accurate at high latitudes, where the losses through nonradiative mechanisms (the solar wind and thermal conduction) play a dominant role.

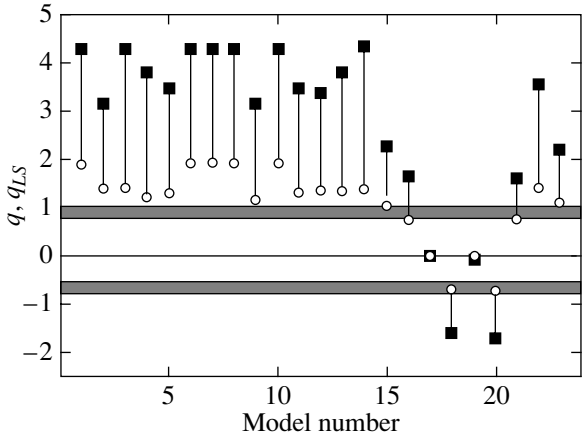

Fig. 4. Comparison of the observed q (regions painted gray) with the calculated q (filled squares) and q_{LS} (open circles).

CONCLUSIONS

The magnetic field is a crucial parameter under the effect of which various coronal structures are formed and physical conditions under which the green line emission emerges are created. These conditions include the temperature at which Fe XIV exists ($\sim$2 MK) and a fairly high density. The thermal regime of the corona is the result of a complex interaction between the mechanisms of matter and energy inflow and outflow.

We showed that the correlation between the coronal green line intensity and the magnetic field strength is different in the sunspot formation zone and the high-latitude zone. The correlation coefficients r_B between these parameters in the two latitude zones vary in antiphase. In the low-latitude zone, the correlation coefficients are always positive, reach their highest values at solar minimum, and decrease significantly at maximum. In the high-latitude zone, the correlation coefficients reach their highest positive values at cycle maximum and negative, but approximately the same (in absolute value) values at minimum.

At solar minimum (when the magnetic field has a relatively simple structure), the correlation between the green line intensity and the magnetic field

strength and its components can be represented by a power law of the type $I \propto B^q$. In the equatorial zone, the power-law index is positive, the green line intensity increases with magnetic field strength. At high latitudes, the green line intensity decreases with increasing magnetic field strength, the power-law index is negative and essentially does not exceed unity in absolute value.

Our results suggest that the mechanisms of matter and energy inflow and outflow and their interaction are different in different latitude zones of the Sun. The conditions for the balance of energy and matter established in the equatorial and polar zones as a result of the interaction between these mechanisms also prove to be different. A large number of dense low loops with a high temperature emerge in the low-latitude zone. The green line here is intense. In the high-latitude zone, regions with an open magnetic configuration dominate, the outflow of matter and energy is enhanced, and a dynamic balance is established at a lower temperature and a considerably lower density than at low latitudes. As the field strength increases near solar minimum, the number of such regions increases and the green line intensity decreases.

Our comparison of the experimental power-law indices q with various theoretical models showed that none of the coronal heating mechanisms considered gave q close to its observed values for all latitudes. In other words, it is not possible to choose a unified mechanism that would adequately describe the balance between the inflow and outflow of matter and energy in the corona at all latitudes. The DC (dissipation of currents) and AC (dissipation of Alfvén and magnetosonic waves) mechanisms probably act simultaneously on the Sun. These mechanisms can lead to values of q with the opposite sign. The simultaneous action of these two mechanisms can cause an effective decrease in the absolute value of q compared to its theoretical values for each of these mechanisms. The contribution from DC and AC depends on the structure and spatial sizes of the emitting region and on the magnetic field strength; it varies with latitude and cycle phase.

Our results indicate that at cycle minimum, when the field structure is simplest, the wave (AC) mechanisms and the current DC mechanisms probably dominate in the high-latitude zone and the sunspot formation zone, respectively.

ACKNOWLEDGMENTS

This work was supported by the Russian Foundation for Basic Research (project no. 05-02-16090).

REFERENCES

1. J. J. Aly and T. Amari, Astron. Astrophys. **319**, 699 (1997).
2. M. J. Aschwanden, *Physics of the Solar Corona: An Introduction* (Springer, Berlin, 2004).
3. O. G. Badalyan and V. N. Obridko, Astron. Zh. **81**, 746 (2004) [Astron. Rep. **48**, 678 (2004)].
4. O. G. Badalyan and V. N. Obridko, Sol. Phys. **238**, 271 (2006).
5. O. G. Badalyan, V. N. Obridko, and J. Sýkora, Astron. Astrophys. Trans. **23**, 555 (2004).
6. O. G. Badalyan, V. N. Obridko, and Yu. Sikora, Astron. Zh. **82**, 535 (2005) [Astron. Rep. **49**, 477 (2005)].
7. M. A. Berger, Astron. Astrophys. **252**, 369 (1991).
8. M. A. Berger, Phys. Rev. Lett. **70**, 705 (1993).
9. P. K. Browning and E. R. Priest, Astron. Astrophys. **159**, 129 (1986).
10. P. Dmitruk and D. O. Gómez, Astrophys. J. **484**, L83 (1997).
11. G. Einaudi, M. Velli, H. Politano, and A. Pouquet, Astrophys. J. **457**, L113 (1996).
12. R. Fisher and S. Musman, Astrophys. J. **195**, 801 (1975).
13. K. Galsgaard and A. Nordlund, J. Geophys. Res. **101**, 13 445 (1996).
14. K. Galsgaard and A. Nordlund, J. Geophys. Res. **102**, 219 (1997).
15. L. Golub and J. M. Pasachoff, *The Solar Corona* (Cambridge Univ. Press, 1997).
16. L. Golub, C. Maxson, R. Rosner, et al., Astrophys. J. **238**, 343 (1980).
17. M. Guhathakurta, R. R. Fisher, and R. C. Altrock, Astrophys. J. **414**, L145 (1993).
18. M. Guhathakurta, R. Fisher, and K. Strong, Astrophys. J. **471**, L69 (1996).
19. G. Halberstadt and J. P. Goedbloed, Astron. Astrophys. **301**, 559 (1995).
20. D. L. Hendrix, G. Van Hoven, Z. Mikić, and D. D. Schnack, Astrophys. J. **470**, 1192 (1996).
21. J. Heyvaerts and E. R. Priest, Astron. Astrophys. **137**, 63 (1984).
22. J. Heyvaerts and E. R. Priest, Astrophys. J. **390**, 297 (1992).
23. J. T. Hoeksema, *Solar Magnetic Fields—1985 through 1990* (Report CSSA-ASTRO-91-01, Center for Space Science and Astronomy, Stanford University, 1991).
24. J. T. Hoeksema and P. H. Scherrer, *The Solar Magnetic Fields—1976 through 1985* (WDCA Report UAG-94, NGDC, Boulder, 1986).
25. J. V. Hollweg, *Advances in Space Plasma Physics*, Ed. by B. Buti (World Sci., Singapore, 1985), p. 77.
26. G. W. Inverarity and E. R. Priest, Astron. Astrophys. **296**, 395 (1995a).
27. G. W. Inverarity and E. R. Priest, Astron. Astrophys. **302**, 567 (1995b).
28. G. W. Inverarity, E. R. Priest, and J. Heyvaerts, Astron. Astrophys. **293**, 913 (1995).
29. A. P. Kharshiladze and K. G. Ivanov, Geomagn. Aéron. **34**, 22 (1994).

30. J. A. Klimchuk, Astron. Soc. Pac. Conf. Ser. **277**, 321 (2002).
31. J. A. Klimchuk and L. J. Porter, Nature **377**, 131 (1995).
32. V. Letfus, L. Kulčár, and J. Sýkora, *Solar and Interplanetary Dynamics,* Ed. by M. Dryer and E. Tandberg-Hanssen (Reidel, Dordrecht, 1980), p. 49.
33. C. H. Mandrini, J. Démoulin, and A. Klimchuk, Astrophys. J. **530**, 999 (2000).
34. L. J. Milano, D. O. Gómez, and P. C. H. Martens, Astrophys. J. **490**, 442 (1997).
35. S. A. Mitchell, *Handbuch der Astrophysik,* Ed. by G. Eberhard, A. Kohlschütter, and H. Ludendorff (Springer, Berlin, 1929), Vol. 4, p. 231.
36. V. N. Obridko and B. D. Shelting, Sol. Phys. **184**, 187 (1999).
37. L. Ofman, J. M. Davila, and R. S. Steinolfson, Astrophys. J. **444**, 471 (1995).
38. E. N. Parker, Astrophys. J. **264**, 642 (1983).
39. E. N. Parker, Astrophys. J. **330**, 474 (1988).
40. M. S. Ruderman, D. Berghmans, M. Goosens, and S. Poedts, Astron. Astrophys. **320**, 305 (1997).
41. V. Rušin and M. Rybanský, Sol. Phys. **207**, 47 (2002).
42. C. J. Schrijver, A. W. Sandman, M. J. Aschwanden, and M.L. DeRosa, in *Proceedings of the 13th Cambridge Workshop on Cool Stars, Stellar Systems and the Sun,* Ed. by F. Favata, G. A. J. Hussian, and B. Battrick (ESA, Noordvijk, 2004), ESA SP-560, p. 65.
43. M. Storini and J. Sýkora, Nuovo Cimento **20C**, 923 (1997).
44. P. A. Sturrock and Y. Uchida, Astrophys. J. **246**, 331 (1981).
45. J. Sýkora, Bull. Astron. Inst. Czech. **22**, 12 (1971).
46. J. Sýkora, Sol. Phys. **140**, 379 (1992).
47. J. Sýkora and J. Rybák, Adv. Space Res. **35**, 393 (2005).
48. P. Ulmschneider, *The Physics of Chromospheres and Coronae,* Ed. by H. M. Antia, A. Bhatnagar, and P. Ulmschneider (Springer, Heidelberg, 2003), p. 232.
49. A. A. van Ballegooijen, Astrophys. J. **311**, 1001 (1986).
50. G. E. Vekstein, E. R. Priest, and C. D. C. Steele, Astrophys. J. **417**, 781 (1993).
51. Y.-M. Wang, N. R. Sheeley, Jr., S. H. Hawley, et al., Astrophys. J. **485**, 419 (1997).
52. H. P. Warren and A. R. Winebarger, Astrophys. J. **645**, 711 (2006).

Translated by V. Astakhov